Andreas Enzenhöfer
Department of Mechanical Engineering,
Centre for Intelligent Machines,
McGill University,
Montréal, QC H3A 0C3, Canada;
CM Labs Simulations,
Montréal, QC H3C 1T3, Canada

Albert Peiret
Department of Mechanical Engineering,
Centre for Intelligent Machines,
McGill University,
Montréal, QC H3A 0C3, Canada

Marek Teichmann
CM Labs Simulations,
Montréal, QC H3C 1T3, Canada

József Kövecses
Department of Mechanical Engineering,
Centre for Intelligent Machines,
McGill University,
Montréal, QC H3A 0C3, Canada

A Unit-Consistent Error Measure for Multibody Systems With Unilateral Constraints

Modeling multibody systems subject to unilateral contacts and friction efficiently is challenging, and dynamic formulations based on the mixed linear complementarity problem (MLCP) are commonly used for this purpose. The accuracy of the MLCP solution method can be evaluated by determining the error introduced by it. In this paper, we find that commonly used MLCP error measures suffer from unit inconsistency leading to the error lacking any physical meaning. We propose a unit-consistent error measure, which computes energy error components for each constraint dependent on the inverse effective mass and compliance. It is shown by means of a simple example that the unit consistency issue does not occur using this proposed error measure. Simulation results confirm that the error decreases with convergence toward the solution. If a pivoting algorithm does not find a solution of the MLCP due to an iteration limit, e.g., in real-time simulations, choosing the result with the least error can reduce the risk of simulation instabilities and deviation from the reference trajectory. [DOI: 10.1115/1.4042690]

1 Introduction

There are numerous issues that make multibody dynamics simulations with contacts and friction challenging. Many applications in engineering and related fields impose strict requirements on the computational time available for each time-step and on the accuracy of the simulation, such as in real-time simulations. Accurate solutions and low computational time usually cannot be obtained simultaneously. Contact in multibody systems can be modeled through unilateral constraints. This often results in a dynamic formulation that can mathematically be described as a linear complementarity problem (LCP) or mixed linear complementarity problem (MLCP). There is a wide range of algorithms in the literature to solve LCPs and MLCPs, which can be classified into two types: direct and iterative methods [1]. Generally, iterative solvers are computationally more efficient than direct ones. Nevertheless, only direct solvers are able to deliver the exact solution of the MLCP given enough computational time. It is not an easy task to choose the solver that best suits the problem at hand, especially when there is a time constraint so that a solution with the desired tolerance cannot be found. In this case, the simulation accuracy can be increased significantly if we measure the error of all computed solutions throughout the solver iterations and choose the solution with the least error.

Simulations of mechanical systems are approximations of reality that involve the creation of a model where some details are always neglected. This can lead to errors in the system behavior obtained through simulations compared to the real mechanical system. We call the error introduced by modeling approximations the *modeling error*. In simulations, continuous time is approximated by discrete time intervals. Then, the system configuration, motion, and reaction forces are evaluated at a discrete time. This leads to an error due to time discretization, termed *discretization error*. Models subject to unilaterality can lead to an MLCP formulation, which gives rise to an error introduced by the MLCP solver, the *solver error*. In this paper, we do not intend to measure the modeling or discretization error of the simulation but the solver error only.

In multibody dynamics benchmarking, González et al. [2] define the solution accuracy as the relative position error between the given reference solution and the computed solution at a discrete point in time. The overall simulation error is obtained by aggregation of the position errors over the simulation time. González et al. [3] extend this approach by introducing an energy error measure for conservative systems to avoid large position errors in case of a small phase error. However, this energy error is not applicable to nonconservative systems since the mechanical energy at the beginning of the simulation is used as the Ref. [3]. In robotics, Erez et al. [4] compare the numerical integration errors of dynamics engines of different simulation platforms by monitoring the deviation of the system configuration from a reference trajectory. This reference trajectory is obtained by reducing the integration time-step size and therefore the integration error. All error measures and metrics in the aforementioned papers [2–4] require a reference solution. This limits the possible applications significantly since such reference solutions are not always trivial to obtain and certainly cannot be computed in real time for interactive simulations.

In finite element analysis, the literature on a posteriori error estimation is vast. A posteriori error estimation uses the computed solution itself to assess the simulation accuracy [5]. Thus, no reference solution is required. Babuška and Rheinboldt [6,7] propose error estimation techniques, which approximate the energy norm of each finite element. These are commonly used for adaptive meshing techniques [8]. Babuška et al. [9] validate a posteriori error estimation in terms of performance and robustness. A summary of a posteriori error estimation can be found in Refs. [5] and [10]. We refer the reader to Ref. [11] for an introduction to finite element methods including error estimation.

The mathematics literature contains numerous papers and books about the theory of error bounds of complementarity problems (CP), i.e., the general problem formulation containing the LCP, MLCP, and nonlinear complementarity problem. Pang [12,13] defines the natural residual as the componentwise minimum between the CP solution vector and the slack vector, which are supposed to be complementarity to each other. This residual can be used to measure the closeness of the computed result to

Contributed by the Design Engineering Division of ASME for publication in the Journal of Computational and Nonlinear Dynamics. Manuscript received October 31, 2018; final manuscript received January 15, 2019; published online February 15, 2019. Assoc. Editor: Paramsothy Jayakumar.

being a solution of the CP. Mangasarian and Shiau [14] propose another natural residual specifically for cases where Pang's residual function fails to bound the errors. Their natural residual definition has been replaced by an improved error bound consisting of two natural residuals in combination [15]. Merit functions for the CP are used to design globally convergent solution algorithms and serve also as error bounds. Fukushima [16] discusses several merit functions one of which is the Fischer-Burmeister function. This function is defined by the componentwise difference between the ℓ_2-norm and the ℓ_1-norm of two components of the solution and slack vector. The Fischer-Burmeister merit function is commonly used in iterative algorithms to capture the error in rigid body simulations [17–19]. Lu and Trinkle [20] measure the error in a potential solution given by the algorithm by using the Chen–Chen–Kanzow reformulation function, which also depends on the Fischer-Burmeister function. Lacoursière et al. [21] introduced multiple quality metrics, which do not only measure the MLCP solver error but also the contact penetration error as well as the error in the friction force magnitude and alignment with the sliding direction. It is not in the scope of this present paper to determine and evaluate the error in the dynamic formulation, the objective is to measure the MLCP solver error only.

The great advantage of the aforementioned residual and merit functions for the CP is that the non-negativity and complementarity conditions are used to determine the error in the computed result. Thus, no reference solution is required. Furthermore, the error can be computed relatively inexpensively in every algorithm iteration. This is advantageous because we can keep track of the solver error throughout the iterations. Then, the intermediate solution with the least error can be chosen in case the solver does not terminate due to an iteration limit. However, these error functions have a major drawback if used for mechanical problems. They do not take the physical nature of the solution vector (forces or impulses) and the slack vector (accelerations or velocities) into consideration. Thus, the computed errors are unit inconsistent and have no physical meaning.

In this paper, we introduce two commonly used error measures based on the natural residual [13] and the Fischer-Burmeister function [16]. We show that these approaches do not take the nature of the model into account and can suffer from physical inconsistency. In other words, the units of the physical quantities these error measures are based on are ignored during their computation so that the resultant error does not represent any physical quantity. Furthermore, we present a unit-consistent energy error measure for MLCP solvers that does not require any reference solution and can be efficiently computed for every solver iteration in order to improve simulation accuracy. Finally, we apply this proposed error measure to monitor the quality of the intermediate results in an engineering simulation at each iteration of a direct solver and choose the best solution if the algorithm does not terminate.

2 Multibody Dynamics With Contact

Let us consider a multibody system with the generalized velocities $\mathbf{v} \in \mathbb{R}^{6m}$ for m rigid bodies and the transformation $\mathbf{Jv} = \mathbf{w}$ that defines the constraint subspace where $\mathbf{w} \in \mathbb{R}^n$ represents the velocities in that subspace and $\mathbf{J} \in \mathbb{R}^{n\times 6m}$ is the constraint Jacobian. The dynamic equations using a finite difference approximation for the generalized accelerations $\dot{\mathbf{v}} \approx ((\mathbf{v}^+ - \mathbf{v})/h)$ and constraint regularization can be written as [22]

$$\begin{bmatrix} \mathbf{M} & -\mathbf{J}^{\mathrm{T}} \\ \mathbf{J} & \mathbf{C} \end{bmatrix} \begin{bmatrix} \mathbf{v}^+ \\ h\boldsymbol{\lambda}^+ \end{bmatrix} + \begin{bmatrix} -\mathbf{p} \\ h_{-1}\boldsymbol{\Phi} \end{bmatrix} = \begin{bmatrix} \mathbf{0} \\ \mathbf{w} \end{bmatrix} \tag{1}$$

where h is the time-step size, $\mathbf{v}^+$ are the unknown velocities at the end of the step, $\mathbf{v}$ are the known velocities at the beginning of the step, $\mathbf{M} \in \mathbb{R}^{6m\times 6m}$ is the mass matrix, and $\mathbf{p} = \mathbf{Mv} + h\mathbf{f}_a \in \mathbb{R}^m$ combines the momentum and impulse dependent on the generalized applied forces $\mathbf{f}_a$. The limits on the constraint reactions $\boldsymbol{\lambda}^+ \in \mathbb{R}^n$ are specified by the nature of the constraint, e.g., $\lambda_{\mathrm{n}}^+ \geq 0$ for a normal contact force, and $\lambda_{\mathrm{t}}^+ \in [-\mu\lambda_{\mathrm{n}}, +\mu\lambda_{\mathrm{n}}]$ for a friction force component if the box friction approximation [22,23] is used, where λ_n can be an estimate of the normal force from the previous time-step. This removes the dependency between normal and friction forces of the same time-step. In the box friction model, the friction cone is approximated as a polyhedral cone using one normal and two friction directions. The objective of this present paper is not to develop an accurate friction formulation but to measure the error in a given model formulated as an MLCP. The constraints can be regularized through representation of the reaction forces by constitutive relations in implicit form, i.e., $\lambda_i^+ = -k_i\phi_i^+$, where k_i is the constraint stiffness and ϕ_i^+ is the constraint violation at the end of the time-step. This introduces the compliance matrix $\mathbf{C} = \mathrm{diag}\{(1/(k_1h^2)), \ldots, (1/(k_nh^2))\} \in \mathbb{R}^{n\times n}$ and the constraint violation vector $\boldsymbol{\Phi} = [\phi_1 \ldots \phi_n]^{\mathrm{T}} \in \mathbb{R}^n$. Note that the constraint violations of the next time-step are approximated via a finite difference so that the constraint reactions are defined in terms of the unknown velocities. This makes the constraint forces implicit and adds damping to the system, which increases the stability of the formulation.

2.1 Mixed Linear Complementarity Problem.

The general form of the MLCP that needs to be solved at each step is

$$\mathbf{Ax} + \mathbf{b} = \mathbf{w} \tag{2}$$

$$\mathbf{0} \leq \mathbf{u} - \mathbf{x} \perp \mathbf{w}_- \geq \mathbf{0} \tag{3}$$

$$\mathbf{0} \leq \mathbf{x} - \boldsymbol{l} \perp \mathbf{w}_+ \geq \mathbf{0} \tag{4}$$

where $\mathbf{A} = \mathbf{JM}^{-1}\mathbf{J}^{\mathrm{T}} + \mathbf{C}$ is the lead matrix, $\mathbf{b} = \mathbf{JM}^{-1}\mathbf{p} + (1/h)\boldsymbol{\Phi}$ is called parameter vector, and the variables $\mathbf{x} = h\boldsymbol{\lambda}^+ \in [\boldsymbol{l}, \mathbf{u}]$ are the constraint impulses subject to lower and upper bounds $\boldsymbol{l}$ and $\mathbf{u}$. The non-negative components of the constraint-space velocity (also known as slack variables) $\mathbf{w} = \mathbf{w}_+ - \mathbf{w}_-$ are complementary to the saturation of the lower and upper bounds, denoted by the operator $\perp$. Therefore, the slack variable is positive ($w_{+,i} > 0$) if the main variable x_i is at the lower bound ($x_i = l_i$). Likewise, the slack variable is negative ($w_{-,i} > 0$) if the main variable x_i is at the upper bound ($x_i = u_i$).

2.2 Solver Algorithms.

There are two main types of algorithms for solving an MLCP: *direct* and *iterative* methods [1]. Direct methods, also known as *pivoting methods*, try to determine the set of variables that are at the upper or lower bound, or within the bounds. They start with an initial guess for these index sets in order to solve for the unknown variables. If the guess does not lead to a solution of the MLCP, the index sets are modified by systematically swapping variables from one set to another until a solution is reached. Unfortunately, there is no guarantee that the result in an iteration is closer to the solution than the previous result.

In contrast to direct methods, iterative methods do not make assumptions on index sets nor solve directly for the unknown variables. Instead, convergence is reached by improving the solution in every iteration. Then, each iterate is closer to the solution than the previous one if the solver is convergent for the problem at hand. In order to solve the MLCP, direct and iterative solution algorithms perform a series of iterations and compute intermediate solutions, which satisfy Eq. (2). Therefore, the solver error occurs only in the conditions in Eqs. (3) and (4). Note that there are also methods, which do not satisfy Eq. (2) for intermediate solutions, e.g., Lemke's algorithm [1]. For these methods, the error measures presented in this paper cannot be used to determine the closeness of intermediate solutions of being a solution of the MLCP.

3 Existing Error Measures

In Secs. 3.1 and 3.2, we present two functions that can be used to measure the solver error per constraint based on the MLCP solution $\mathbf{x}$ and slack variable $\mathbf{w}$. If Eq. (2) is satisfied, the variable x_i represents the constraint reaction impulse, and its slack variable w_i represents the constraint velocity. However, for an intermediate solution before the algorithm converges, the feasibility of the impulses ($x_i \in [l_i, u_i]$) and the constraint velocities ($w_{+,i} \geq 0$, $w_{-,i} \geq 0$) as well as their complementarity ($w_{+,i}(x_i - l_i) = 0$, $w_{-,i}(u_i - x_i) = 0$) may not be guaranteed.

3.1 Fischer-Burmeister Error Function. For the MLCP in Eqs. (2)–(4), two Fischer-Burmeister error functions associated with the upper and lower bounds can be introduced per constraint i [16,24]

$$\begin{aligned} \psi_{\mathrm{FB},u,i} &= (u_i - x_i) + w_{-,i} - \sqrt{(u_i - x_i)^2 + w_{-,i}^2} \\ \psi_{\mathrm{FB},l,i} &= (x_i - l_i) + w_{+,i} - \sqrt{(x_i - l_i)^2 + w_{+,i}^2} \end{aligned} \tag{5}$$

We take the maximum of the absolute values resulting from Eq. (5) to obtain one error value for constraint i

$$\delta\psi_{\mathrm{FB},i} = \max(|\psi_{\mathrm{FB},l,i}|, |\psi_{\mathrm{FB},u,i}|) \tag{6}$$

Figure 1 visualizes isoline plots for the Fischer-Burmeister technique in Eq. (6) for contact and friction. Given $\delta\psi_{\mathrm{FB},i}$, we can compute an error value for the entire system of equations, called *system error*. The ℓ_1-norm of the component vector $\delta\boldsymbol{\psi}_{\mathrm{FB}} = [\delta\psi_{\mathrm{FB},1} \ldots \delta\psi_{\mathrm{FB},n}]^{\mathrm{T}}$ can be used to define the system error as

$$\delta\psi_{\mathrm{FB}} = ||\delta\boldsymbol{\psi}_{\mathrm{FB}}||_1 = \sum_{i=1}^{n} |\delta\psi_{\mathrm{FB},i}| \tag{7}$$

3.2 Natural Residual. Similar to the approach for the Fischer-Burmeister function, we can introduce two natural residuals associated with the upper and lower bounds per constraint i for an MLCP [12,13]

$$\begin{aligned} \psi_{\mathrm{res},u,i} &= \min(u_i - x_i, w_{-,i}) \\ \psi_{\mathrm{res},l,i} &= \min(x_i - l_i, w_{+,i}) \end{aligned} \tag{8}$$

where the arguments in the minimum function represent the variables in the conditions in Eqs. (3) and (4). We define the error of constraint i as the maximum of the absolute values of the two functions

$$\delta\psi_{\mathrm{res},i} = \max(|\psi_{\mathrm{res},u,i}|, |\psi_{\mathrm{res},l,i}|) \tag{9}$$

Figure 2 shows the isoline plots for contact and friction. The system error can be defined using the ℓ_1-norm

$$\delta\psi_{\mathrm{res}} = ||\delta\boldsymbol{\psi}_{\mathrm{res}}||_1 = \sum_{i=1}^{n} |\delta\psi_{\mathrm{res},i}| \tag{10}$$

where $\delta\boldsymbol{\psi}_{\mathrm{res}} = [\delta\psi_{\mathrm{res},1} \ldots \delta\psi_{\mathrm{res},n}]^{\mathrm{T}}$ is the component vector composed of the errors for all constraints in the system.

3.3 Unit Consistency Issues. The two error measures presented above are commonly used in simulation of multibody systems with contact to estimate the accuracy of the solver algorithm [24,25]. However, these error measures have a significant shortcoming, which is rarely discussed. The different physical nature of the constraint impulses $\mathbf{x}$ and the constraint-space velocities $\mathbf{w}$ is not taken into account. This can lead to unit inconsistencies in the Fischer-Burmeister function. For example, if $u_i - x_i$ and $w_{-,i}$ are simultaneously nonzero, we add impulses expressed in N·s to velocities expressed in m/s, which leads to a sum in Eq. (5) without any physical meaning. Unit inconsistencies in the ℓ_1-norm of the natural residual can also occur if the components of $\delta\boldsymbol{\psi}_{\mathrm{res}}$ contain variables of mixed physical quantities, e.g., impulses expressed in N·s and velocities expressed in m/s. Furthermore, another type of unit inconsistency can occur when the system contains constraints representing restrictions on both, linear and angular motion. Then, $\mathbf{w}$ is composed of a mix of point velocities in m/s and angular velocities in s^{-1}. There is no clear physical meaning of the ℓ_1-norm of $\delta\boldsymbol{\psi}_{\mathrm{res}}$ that mixes impulses, point velocities and angular velocities. Even if all error is exclusively arising in the impulses, i.e., the components of $\delta\boldsymbol{\psi}_{\mathrm{res}}$ carry exclusively impulse units, the effect of such impulse error on the system motion is dependent on the mass of the constrained bodies. For example, a relatively small impulse error may have a more significant impact on the motion of a light body than a relatively large impulse error on the motion of a heavy body.

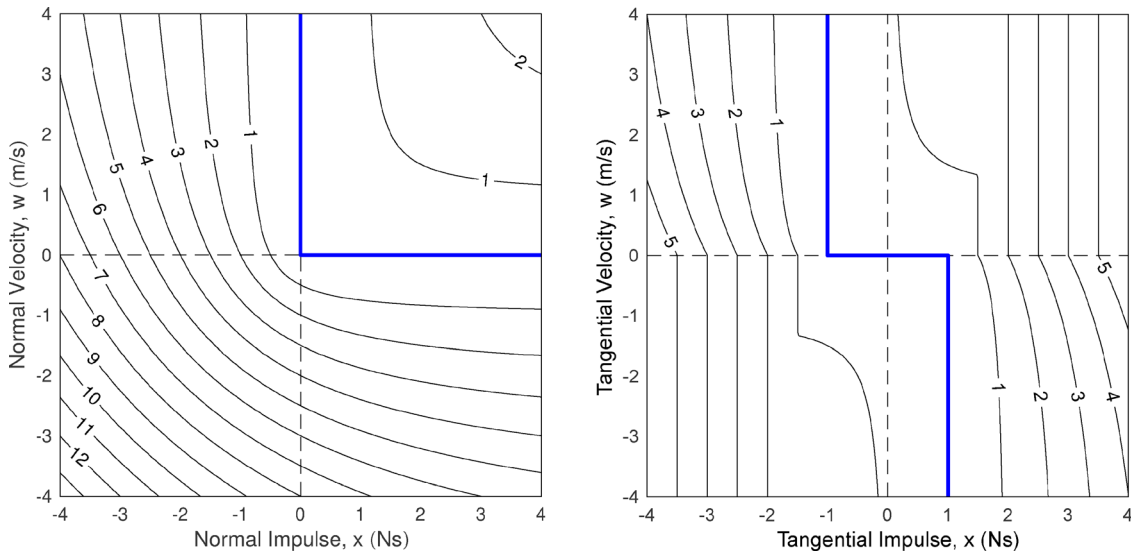

Fig. 1 Fischer-Burmeister error isolines for contact (left, $l_i = 0\,\mathrm{N}\cdot\mathrm{s}$, $u_i = +\infty\,\mathrm{N}\cdot\mathrm{s}$) and friction (right, $l_i = -1\,\mathrm{N}\cdot\mathrm{s}$, $u_i = +1\,\mathrm{N}\cdot\mathrm{s}$). The error is zero on the thick solid line representing the set of valid solutions.

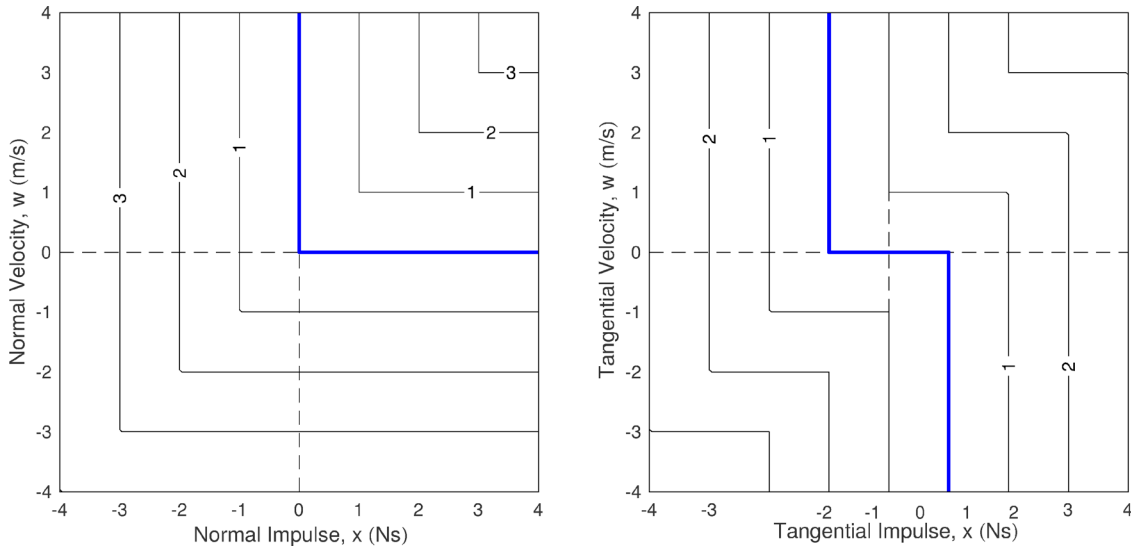

Fig. 2 Natural residual error isolines for contact (left, $l_i = 0\,\mathrm{N}\cdot\mathrm{s}$, $u_i = +\infty\,\mathrm{N}\cdot\mathrm{s}$) and friction (right, $l_i = -1\,\mathrm{N}\cdot\mathrm{s}$, $u_i = +1\,\mathrm{N}\cdot\mathrm{s}$). The error is zero on the thick solid line representing the set of valid solutions.

4 Unit-Consistent Error Measure

In this section, we present a novel error measure that defines the solver error as a function of the MLCP solution vector $\mathbf{x}$ and the slack vector $\mathbf{w}$. This error measure is unit consistent in all the critical scenarios outlined in Sec. 3.3. Unit consistency is guaranteed through multiplication with a mass or inertia quantity, an approximation of the *effective mass or inertia* associated with each constraint. Then, we obtain constraint error components expressed in energy units, which allows us to easily combine and compare them.

4.1 Effective Mass. We consider a system of m rigid bodies connected by n bilateral and unilateral constraints. The system mass matrix is given by $\mathbf{M} \in \mathbb{R}^{6m\times 6m}$ and the system constraint Jacobian by $\mathbf{J} \in \mathbb{R}^{n\times 6m}$ where the Jacobian row $\mathbf{J}_i \in \mathbb{R}^{1\times 6m}$ corresponds to constraint i. Under the assumption that all unilateral constraints are active, i.e., $\mathbf{w} = \mathbf{0}$, the *effective mass element* $\bar{m}_{\mathrm{eff},i}$ associated with constraint i in the constrained multibody system can be defined as [26,27]

$$\bar{m}_{\mathrm{eff},i} = \{(\mathbf{J}\mathbf{M}^{-1}\mathbf{J}^{\mathrm{T}})^{-1}\}_{ii} \tag{11}$$

where $\{\cdot\}_{ii}$ is the ith diagonal element of the matrix in the curly brackets. For large-scale systems, it is very expensive to compute the effective mass matrix, which is the inverse of $\mathbf{J}\mathbf{M}^{-1}\mathbf{J}^{\mathrm{T}}$. However, if $\mathbf{J}\mathbf{M}^{-1}\mathbf{J}^{\mathrm{T}}$ is diagonally dominant, i.e., $\{\mathbf{J}\mathbf{M}^{-1}\mathbf{J}^{\mathrm{T}}\}_{ii} > \sum_{i\neq j}|\{\mathbf{J}\mathbf{M}^{-1}\mathbf{J}^{\mathrm{T}}\}_{ij}|$, the effective mass element $\bar{m}_{\mathrm{eff},i}$ can be approximated as

$$m_{\mathrm{eff},i} = \left\{(\mathbf{J}\mathbf{M}^{-1}\mathbf{J}^{\mathrm{T}})_{ii}\right\}^{-1} = \frac{1}{\mathbf{J}_i\mathbf{M}^{-1}\mathbf{J}_i^{\mathrm{T}}} \tag{12}$$

The less coupling between the constraints in the multibody system, the better is this approximation. The approximated effective mass element $m_{\mathrm{eff},i}$ is equivalent to the effective mass element $\bar{m}_{\mathrm{eff},i}$ in the case where the system fully decouples, and it is smaller otherwise, i.e., $m_{\mathrm{eff},i} \leq \bar{m}_{\mathrm{eff},i}$ (see the Appendix). Thus, only the mass and inertia effects of directly adjacent bodies are taken into consideration and no other constraints between these bodies are regarded. For a long chain of bodies connected by spherical joints, the approximated effective mass of a constraint only contains contributions of the two bodies, which are linked to each other by constraint i. For two bodies connected by multiple constraints, e.g., a cube in contact with a plane, the approximated effective mass of constraint 1 does not receive any contribution of constraint 2 even if the same bodies are involved. This approximation of the effective mass element has been made to keep the computational cost low. Therefore, the solver error can be computed for every iteration without significant impact on the solver performance.

The MLCP lead matrix $\mathbf{A}$ in Eq. (2) is defined as the sum of the inverse effective mass matrix $\mathbf{J}\mathbf{M}^{-1}\mathbf{J}^{\mathrm{T}}$ and the diagonal regularization matrix $\mathbf{C}$. Then, the diagonal elements a_{ii} of $\mathbf{A}$ can be written as

$$a_{ii} = \frac{1}{m_{\mathrm{eff},i}} + c_i \tag{13}$$

where element c_i is the diagonal element of $\mathbf{C}$ and represents the compliance of constraint i, which is usually small and it can also be set to zero if the constraints are not redundant. The element a_{ii} combines the inverse of the approximated effective mass with the constraint compliance. It carries inverse mass units kg^{-1} if the translational motion is constrained or inverse inertia units $(\mathrm{kg\,m^2})^{-1}$ if the angular motion is restricted by constraint i. In the following sections, a_{ii} will simply be referred to as *inverse effective mass* element, which is given without any additional computations as the diagonal element of $\mathbf{A}$.

4.2 Energy Error Measure. Given a solution $\mathbf{x}$ of the MLCP problem in Eq. (2), the ith component can be decomposed into

$$x_i = x_{0,i} + \delta x_{u,i} - \delta x_{l,i} \tag{14}$$

where the feasible component $x_{0,i} \in [l_i, u_i]$. The other components are defined as

$$\begin{aligned} \delta x_{u,i} &= \max(x_i - u_i, 0) \\ \delta x_{l,i} &= \max(l_i - x_i, 0) \end{aligned} \tag{15}$$

which quantify the violation of the upper and lower bounds, respectively. On the other hand, the slack variable $\mathbf{w} = \mathbf{A}\mathbf{x} + \mathbf{b}$ is decomposed into the two non-negative components as

$$w_i = w_{+,i} - w_{-,i} \tag{16}$$

where $w_{+,i} \geq 0$ and $w_{-,i} \geq 0$. Furthermore, we define the saturation of the upper and lower bound as

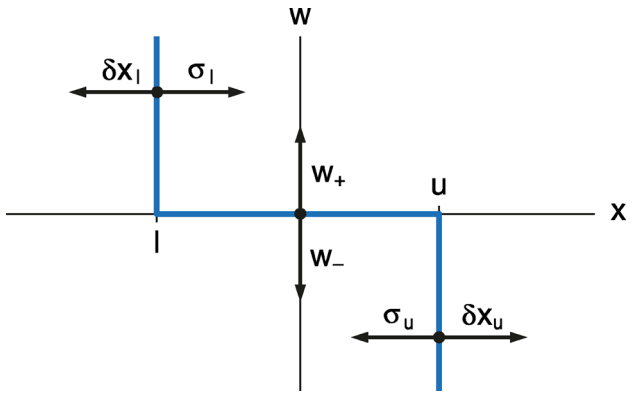

Fig. 3 Decomposition of the constraint impulse x_i and velocity w_i into upper impulse error δx_u, lower impulse error δx_l, positive sliding velocity w_+, negative sliding velocity w_-, upper bound saturation σ_u, and lower bound saturation σ_l

$$\begin{aligned} \sigma_{u,i} &= u_i - (x_{0,i} - \delta x_{l,i}) \\ \sigma_{l,i} &= (x_{0,i} + \delta x_{u,i}) - l_i \end{aligned} \tag{17}$$

The decomposition of x_i and w_i is illustrated for friction in Fig. 3.

We define the upper impulse energy error $\delta e_{x_u,i}$, the lower impulse energy error $\delta e_{x_l,i}$, the positive velocity energy error $\delta e_{w_+,i}$, and the negative velocity energy error $\delta e_{w_-,i}$ as

$$\delta e_{x_u,i} = \frac{1}{2} a_{ii} \delta x_{u,i}^2 \tag{18}$$

$$\delta e_{x_l,i} = \frac{1}{2} a_{ii} \delta x_{l,i}^2 \tag{19}$$

$$\delta e_{w_+,i} = \min\left(\frac{1}{2a_{ii}} w_{+,i}^2, \frac{1}{2} a_{ii} \sigma_{l,i}^2\right) \tag{20}$$

$$\delta e_{w_-,i} = \min\left(\frac{1}{2a_{ii}} w_{-,i}^2, \frac{1}{2} a_{ii} \sigma_{u,i}^2\right) \tag{21}$$

Then, we define the energy error for constraint i as the maximum of the four non-negative energy error components $\delta e_{x_u,i}$, $\delta e_{x_l,i}$, $\delta e_{w_+,i}$, and $\delta e_{w_-,i}$

$$\delta e_i = \max(\delta e_{x_u,i}, \delta e_{x_l,i}, \delta e_{w_+,i}, \delta e_{w_-,i}) \tag{22}$$

Equation (22) is always unit consistent since all components in the maximum function are expressed in Joules.

Figure 4 illustrates isoline plots of the unit-consistent energy error δe_i in the x–w-plane. The thick solid line represents the set of valid solution that have zero error $\delta e_i = 0$, i.e., they satisfy Eqs. (3) and (4). The thin solid lines correspond to sets of solutions with the same error δe_i. The dashed lines are parallel to the line described by the decoupled constraint equation $a_{ii}x_i + b_i = w_i$. The slope of these lines equals the inverse effective mass element a_{ii}. The error increases quadratically along these lines.

Finally, the total error of the system can be defined as the ℓ_1-norm

$$\delta e = ||\delta \mathbf{e}||_1 = \sum_{i=1}^{k} |\delta e_i| \tag{23}$$

given a component vector $\delta \mathbf{e} = [\delta e_1 \ldots \delta e_n]^{\mathrm{T}}$ composed of the constraint errors δe_i. We choose the ℓ_1-norm to simply add up all energy constraint errors. The units are always consistent since all components of $\delta \mathbf{e}$ carry energy units.

Note that this unit-consistent error measure is a problem scaling approach where the inverse effective mass elements a_{ii} are the scaling factor required to obtain unit consistency of all elements of $\delta \mathbf{e}$. It is possible to select different mass or length scaling factors [28] and create error definitions based on different physical quantities, such as momentum or velocity.

4.2.1 Computational Complexity. This section outlines the computational complexity of the error measure with respect to the overall complexity of a direct solver, for which the proposed error measure was originally developed. For direct solvers, the MLCP lead matrix $\mathbf{A}$ is explicitly formed so that its diagonal elements a_{ii} are known [29]. Furthermore, all impulse and velocity components x_i and w_i are always computed since the algorithm must verify if they satisfy the bounds. Then, the components $\delta x_{u,i}$, $\delta x_{l,i}$, $w_{+,i}$, and $w_{-,i}$ are deduced using minimum and maximum functions. The computations of $\delta e_{x_u,i}$, $\delta e_{x_l,i}$, $\delta e_{w_+,i}$, $\delta e_{w_-,i}$, and δe_i require a combination of floating point operations and minimum as well as maximum function. This has to be done for n variables per iteration and all variables have to be added together, which leads to overall computational complexity of $\mathcal{O}(n)$. A direct solver requires a matrix factorization of complexity $\mathcal{O}(n^3)$ per iteration,

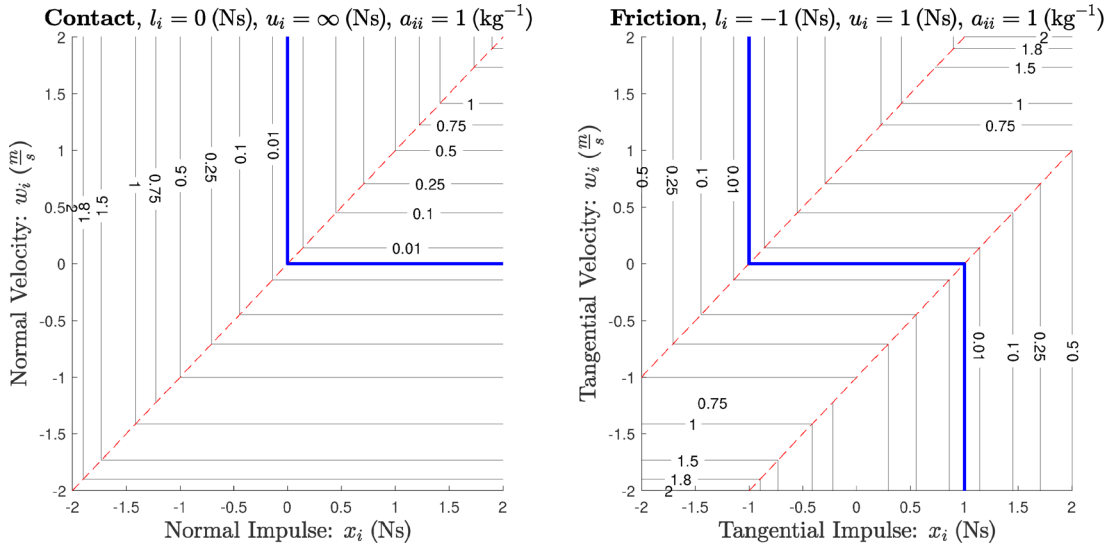

Fig. 4 Energy error isolines for a contact constraint with $l_i = 0$ and $u_i = +\infty$ (left) and a friction constraint with $l_i = -1$ and $u_i = +1$ (right) expressed in Joules. Note that the error is zero on the thick solid line and increases quadratically along the dashed lines.

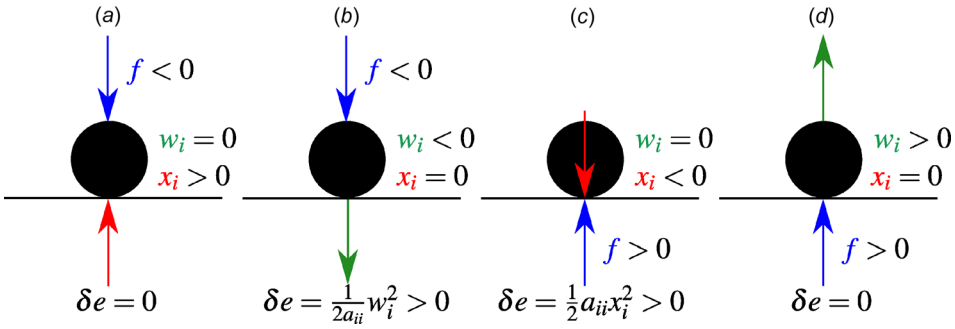

Fig. 5 Single point mass in contact with the ground. There is no energy error for (*a*) and (*d*). The energy error for (*b*) can be interpreted as the kinetic energy generated due to the constraint violation. The energy error in (*c*) equals the kinetic energy that would be released if the impulse was not applied.

which can be sped up to $\mathcal{O}(bn^2)$ for banded matrices with bandwidth b. Thus, the cost of the error measure computation is negligible for large problems.

4.2.2 Interpretation. There are two sources of error: velocity error and impulse error. We consider a single frictionless point mass m_i on the ground with an external force of magnitude $f_a < 0$ applied to it (see Figs. 5(*a*) and 5(*b*)). The dynamic equations for the unilateral constraint with the ground formulated for each time-step can be written in LCP form (see Eqs. (2)–(4)) as

$$a_{ii}x_i + b_i = \frac{1}{m_i}x_i + \frac{hf_a}{m_i} = w_i \qquad (24)$$
$$w_i \geq 0, \quad x_i \geq 0, \quad w_i x_i = 0$$

where the time-step h is constant. The contact impulse x_i and the contact normal velocity w_i must be non-negative and complementary. A direct method assumes one variable to be zero and then computes the solution for the other variable. Under the assumption that the normal velocity is zero $w_i = 0$, the contact impulse is positive $x_i = -(b_i/a_{ii}) = -hf_a > 0$ so that the energy error is zero $\delta e_i = 0$ (see Fig. 5(*a*)). Assuming that the contact impulse is zero $x_i = 0$, the normal velocity is negative $w_i = b_i = (hf_a/m_i) < 0$, which leads to a nonzero energy error $\delta e_i = (1/(2a_{ii}))w_i^2 > 0$ (see Fig. 5(*b*)). This can be interpreted as the kinetic energy that is generated due to the constraint violation. In Figs. 5(*c*) and 5(*d*), we invert the direction of the external force, i.e., $f_a > 0$. Then, we obtain a negative impulse $x_i < 0$ under the assumption that the contact is closed $w_i = 0$ (see Fig. 5(*c*)). This leads to an energy error $\delta e_i = (1/2)a_{ii}x_i^2$, which is equivalent to the kinetic energy that would be released if the impulse was not applied. The error is zero $\delta e = 0$ if we assume detaching contact $x_i = 0$ and $w_i > 0$ (see Fig. 5(*d*)).

4.2.3 Discussion. We consider the motion of a single point mass in positive tangential direction to the ground in Fig. 6. According to the box friction model, this sliding motion is valid only if the friction impulse x_i is equal to the lower bound l_i (see Fig. 6(*a*)). Let us assume that $w_{+,i} > 0$ and $\sigma_{l,i} > 0$ (see Fig. 6(*b*)), then we need to determine whether the friction impulse or the sliding velocity is incorrect, i.e., if the point mass is supposed to stick ($w_{+,i} = 0$) or slide ($\sigma_{l,i} = 0$). If the positive sliding velocity is large $w_{+,i} \gg 0$ and the impulse is close to the lower bound ($\sigma_{l,i}$ is small), it is more likely that the sliding velocity is correct and the impulse should be equal to the lower bound, i.e., $\sigma_{l,i} = 0$. Therefore, a sliding velocity $w_{+,i} > 0$ would not be considered as an error. Then, the overall constraint error is defined to be the minimum of $\delta e_{w_{+,i}} = \min((1/(2a_{ii}))w_{+,i}^2, (1/2)a_{ii}\sigma_{l,i}^2) = (1/2)a_{ii}\sigma_{l,i}^2 > 0$ (see Eq. (20)).

To illustrate why the error is measured in this way, we can consider a straight line parallel to the red dashed line in Fig. 4 (equation line), which contains the point (x_i, w_i) in the x–w-plane. The slope of this line is equal to a_{ii}, and it contains all the solutions that would result from changing the impulse x_i and the velocity w_i according to the relation $w_i = a_{ii}x_i + b_i$. Therefore, from the current solution point, we can adjust the impulse until a solution with no error is reached, i.e., a valid solution on the solid blue line (solution line). One of the two arguments of the minimum function in Eq. (20) becomes zero at the intersection point between the solution line and the equation line. The error component of this argument ($w_{+,i}$ or $\sigma_{l,i}$) is assumed to be incorrect and, thus, determines the energy error. For the point mass example above, this component is the lower-bound saturation $\sigma_{l,i}$.

5 Results

In this section, we present an example for which the existing error measures in Eqs. (7) and (10) are unit inconsistent, whereas the novel energy error measure in Eq. (23) obtains unit-consistent

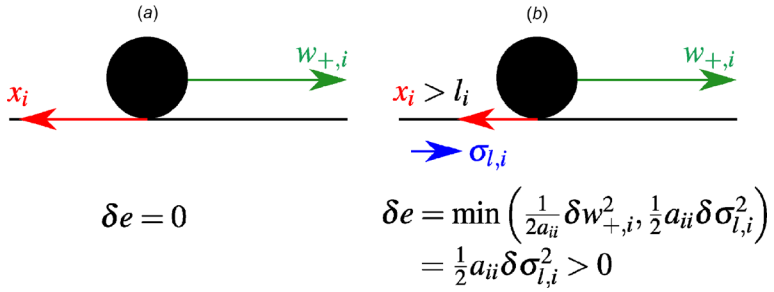

Fig. 6 Single point mass sliding on the ground. There is no error when (*a*) the friction impulse is equal to the lower bound $x_i = l_i$. The error is given by the minimum function in Eq. (20) if $\sigma_{l,i} > 0$ and $w_{+,i} > 0$, i.e., (*b*) due to the friction impulse saturation $\sigma_{l,i}$.

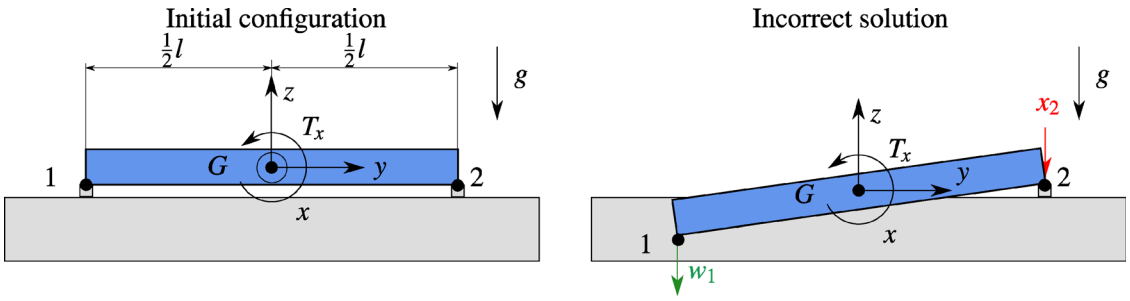

Fig. 7 Rigid rod contacting the ground in two points in its initial configuration before time integration (left) and after time integration using an incorrect solution for the contact impulse x (right)

results. Furthermore, we test the existing error measures and the novel energy error measure for an iterative solver, which computes solutions of MLCPs obtained from a brick wall simulation. We show that the solver error decreases continuously for the novel measure as expected for an iterative solver. Finally, the proposed energy error measure is used in an interactive forklift simulation for the purpose of monitoring intermediate solutions in every iteration of a direct method. We choose the best solution if the method does not converge due to an iteration limit. We show that the usage of an error measure reduces simulation instabilities and deviation from the reference trajectories for direct solvers imposing a limit of the number of iterations.

5.1 Case Study: Rigid Rod on a Plane. We illustrate the unit consistency issue of the existing error measure using a discrete time, frictionless model of a rigid rod, shown in Fig. 7, which is initially at rest, i.e., $\mathbf{v}=\mathbf{0}$. An external moment $T_x=20$ Nm is applied about the center of mass G of the $m=4$ kg heavy rod, which contacts the ground in two points at both ends of the rod under the effect of gravity $g=9.81\,\mathrm{m/s^2}$. The diameter of the rod is negligible with respect to its length of $l=1.5$ m. The constraint Jacobian $\mathbf{J}$, the mass matrix $\mathbf{M}$, and applied forces $\mathbf{f}_a$ are determined to be

$$\mathbf{J}=\begin{bmatrix}0&0&1&-\frac{l}{2}&0&0\\0&0&1&\frac{l}{2}&0&0\end{bmatrix}$$
$$\mathbf{M}=\mathrm{diag}\left\{m\mathbf{E}_{3\times3},\frac{1}{12}ml^2,I_y,\frac{1}{12}ml^2\right\} \tag{25}$$
$$\mathbf{f}_a=\begin{bmatrix}0&0&-mg&T_x&0&0\end{bmatrix}^{\mathrm{T}}$$

where $\mathbf{E}_{3\times3}$ is the 3×3 identity matrix and I_y is small. We assume that the constraints are to be enforced exactly, i.e., there is no constraint relaxation. Given the time-step size $h=0.01$ s, we formulate an LCP to determine the constraint impulses $\mathbf{x}=[x_1,\ x_2]^{\mathrm{T}}$ and constraint-space velocities $\mathbf{w}=[w_1,w_2]^{\mathrm{T}}$ at the two contact points

$$\begin{bmatrix}\frac{4}{m}&-\frac{2}{m}\\-\frac{2}{m}&\frac{4}{m}\end{bmatrix}\begin{bmatrix}x_1\\x_2\end{bmatrix}+\begin{bmatrix}v_z-\frac{l}{2}\omega_x l-h\left(g+\frac{6}{ml}T_x\right)\\v_z+\frac{l}{2}\omega_x l-h\left(g-\frac{6}{ml}T_x\right)\end{bmatrix}$$
$$=\underbrace{\begin{bmatrix}0.1\,\frac{1}{\mathrm{kg}}&-0.5\,\frac{1}{\mathrm{kg}}\\-0.5\,\frac{1}{\mathrm{kg}}&0.1\,\frac{1}{\mathrm{kg}}\end{bmatrix}}_{\mathbf{A}}\underbrace{\begin{bmatrix}x_1\\x_2\end{bmatrix}}_{\mathbf{x}}+\underbrace{\begin{bmatrix}-0.2981\,\frac{\mathrm{m}}{\mathrm{s}}\\0.1019\,\frac{\mathrm{m}}{\mathrm{s}}\end{bmatrix}}_{\mathbf{b}}=\underbrace{\begin{bmatrix}w_1\\w_2\end{bmatrix}}_{\mathbf{w}}$$
$$\mathbf{0}\le\mathbf{x}\perp\mathbf{w}\ge\mathbf{0} \tag{26}$$

where $v_z=0\,\mathrm{m/s}$ and $\omega_x=0\,\mathrm{s^{-1}}$.

We consider a direct method starting with the initial guess $x_1=0$ and $w_2=0$. Then, it follows directly from Eq. (26) that $x_2=-0.1019$ N·s and $w_1=-0.2981\,\mathrm{m/s}$, both of which violate the non-negativity conditions. Physically, x_2 can be interpreted as an adhesive impulse acting in negative z-direction to prevent the contact at point 2 from detaching. This leads to a negative value for w_1, which is the resulting velocity of the rod at contact point 1 so that the rod would penetrate the ground after time integration.

The novel unit-consistent error measure can also be applied to an LCP since this is a special case of the MLCP where $\boldsymbol{l}=\mathbf{0}$ and $\mathbf{u}\to\infty$. Measuring the solver error for this scenario using the Fischer-Burmeister function in Eq. (7) results in $\delta\psi_{\mathrm{FB}}=|\delta\psi_{\mathrm{FB},1}|+|\delta\psi_{\mathrm{FB},2}|=|w_1|+|x_2|=0.2981\,\mathrm{m/s}+0.1019\,\mathrm{N\cdot s}$, where $\delta\psi_{\mathrm{FB},1}$ and $\delta\psi_{\mathrm{FB},2}$ are computed using Eqs. (5) and (6). We can see that $\delta\psi_{\mathrm{FB}}$ has no physical meaning because velocity and impulse components simply cannot be added. It is apparent that this unit inconsistency also occurs if the solver error is determined using the natural residual. The unit-consistent energy error measure overcomes this issue through calculation of the energy error components equivalent to the error in w_1 and x_2. The constraint errors measure the energy error associated with a constraint and can be determined to be $\delta e_1=(1/2a_{11})w_{-,1}^2=4.44\times10^{-2}\,\mathrm{J}$ and $\delta e_2=(1/2)a_{22}\delta x_{l,2}^2=5.2\times10^{-3}\,\mathrm{J}$ using Eqs. (18)–(22). Now, we can compute a unit-consistent system error $\delta e=\delta e_1+\delta e_2=4.96\times10^{-2}\,\mathrm{J}$ using Eq. (23).

5.1.1 Discussion. All the above computations were done using the approximation of the effective mass elements (see Sec. 4.1). The effective mass matrix for the system in Fig. 7 is

$$\mathbf{A}^{-1}=(\mathbf{J}\mathbf{M}^{-1}\mathbf{J}^{\mathrm{T}})^{-1}=\begin{bmatrix}\bar{m}_{\mathrm{eff},1}&\bar{m}_{\mathrm{eff},12}\\\bar{m}_{\mathrm{eff},21}&\bar{m}_{\mathrm{eff},2}\end{bmatrix}=\begin{bmatrix}1.33\,\mathrm{kg}&0.66\,\mathrm{kg}\\0.66\,\mathrm{kg}&1.33\,\mathrm{kg}\end{bmatrix} \tag{27}$$

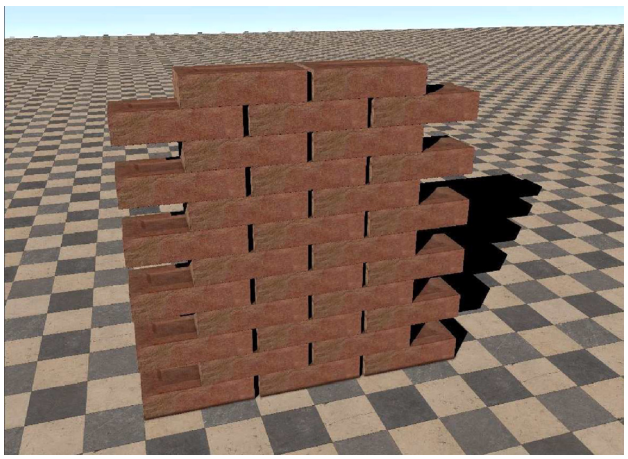

Fig. 8 Brick wall example

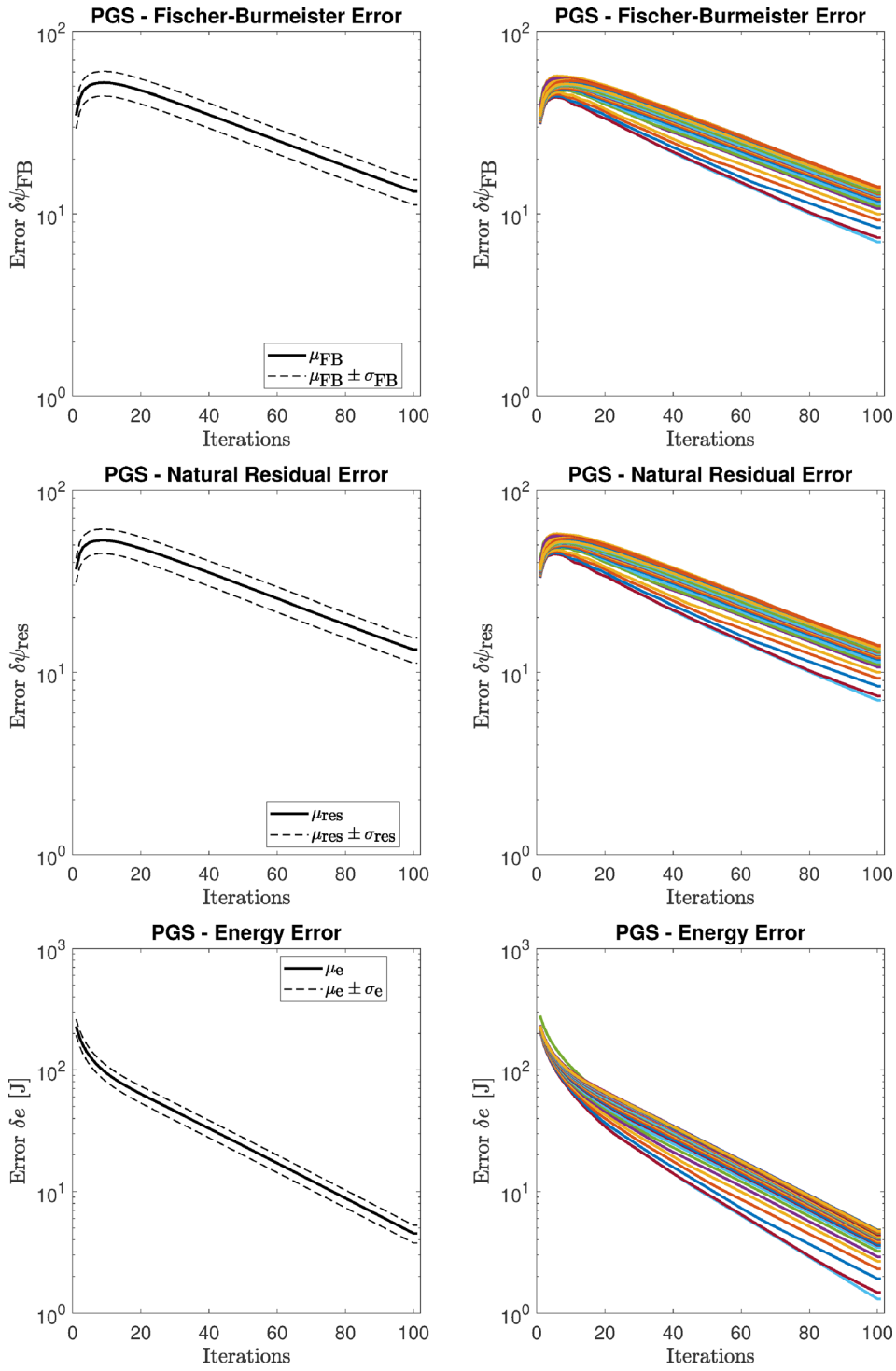

Fig. 9 Brick wall example in Fig. 8 solved by PGS, on the left solid lines illustrate the average errors and the dashed lines the upper and lower error limit given by the average plus or minus the standard deviation, on the right each line represents the iteration–error curve for one time-step

Thus, the approximation of the effective mass $m_{\mathrm{eff},i}$ underestimates the effective mass of the constrained system $\bar{m}_{\mathrm{eff},i}$. The velocity-based energy errors per constraint are $\delta\bar{e}_1 = (1/2)\bar{m}_{\mathrm{eff},1} w^2_{-,1} = 5.91 \times 10^{-2}\,\mathrm{J} > \delta e_1$, i.e., the error is underestimated using the approximated effective mass $m_{\mathrm{eff},i}$. The constraint energy error due to an incorrect impulse is $\delta\bar{e}_2 = (1/(2\bar{m}_{\mathrm{eff},2}))\delta x^2_{l,2} = 3.9 \times 10^{-3}\,\mathrm{J} < \delta e_2$; thus, it is overestimated using the approximated effective mass $m_{\mathrm{eff},i}$. The unit-consistent system error is then $\delta\bar{e} = \delta\bar{e}_1 + \delta\bar{e}_2 = 6.30 \times 10^{-2}\,\mathrm{J} > \delta e$.

We consider the symmetric positive definite LCP lead matrix $\mathbf{A} = \mathbf{J}\mathbf{M}^{-1}\mathbf{J}^{\mathrm{T}} + \mathbf{C}$ where $\mathbf{C} = \mathbf{0}$ in the example above. It is proven in the Appendix that the diagonal elements of the inverse matrix is greater than or equal to the inverse of the diagonal $(\mathbf{A}^{-1})_{ii} \geq (1/\mathbf{A}_{ii})$. Strict equality holds if and only if $\mathbf{A}$ is diagonal, i.e., the constraints in the systems and completely decoupled.

Fig. 10 Forklift driving example

Hence, the approximated effective mass element $m_{\text{eff},i}$ introduced in Sec. 4.1 never overestimates the effective mass element $\bar{m}_{\text{eff},i}$. If the constraints are coupled, as in Fig. 7, velocity-based energy errors are always underestimated using the approximated effective mass, whereas impulse-based energy errors are always overestimated. If there are predominantly impulse-based errors, the total system error will be overestimated; if there are predominantly velocity-based errors, it will be underestimated. Thus, it cannot be generally predicted whether the approximation overestimates or underestimates the total system energy error.

5.2 Discrete Simulation Steps: Brick Wall. We test the novel energy error measure for the example in Fig. 8, which consists of a stack of 30 boxes laid out in a brick wall pattern. The brick wall is 12 bricks tall, and we alternate between rows of two or three bricks in width. Furthermore, there are small lateral gaps between two adjacent bricks. We use a direct solver to accurately simulate the wall behavior and store an MLCP for each of the 500 time steps. Then, the projected Gauss–Seidel (PGS) iterative method is used to find a solution of all of these MLCPs with 100 solver iterations for each time-step. Iterative solvers are known to converge to a solution by continuously improving the solution with every iteration. Hence, we expect the error to decrease with the number of iterations. Note that it is possible that iterative solvers do not converge to the solution. This depends on the physical problem and the mathematical properties of the MLCP lead matrix. Convergence is guaranteed only if matrix $\mathbf{A}$ is diagonally dominant.

Figure 9 shows the results for the solver error per iteration defined by the Fischer-Burmeister error measure $\delta\psi_{\text{FB}}$, the natural residual error measure $\delta\psi_{\text{res}}$, and the proposed energy error measure δe. Only the latter treats physical units consistently. The set of results contains the solver error per iteration for $\bar{T} = 500$ time steps for which we compute the average error and the standard deviation. The average energy error per time-step μ_{e} is defined as

$$\mu_{\text{e}} = \frac{1}{\bar{T}} \left(\sum_{k=1}^{\bar{T}} \delta e(t_k) \right) \tag{28}$$

where $\delta e(t_k)$ is the energy error at time t_k, and the standard deviation of the energy error σ_{e} is given as

$$\sigma_{\text{e}} = \sqrt{\frac{1}{\bar{T}-1} \left(\sum_{k=1}^{\bar{T}} \{\delta e(t_k) - \mu_e\}^2 \right)} \tag{29}$$

The average and standard deviation for the Fischer-Burmeister and natural residual solver errors can also be calculated using this approach by replacing $\delta e(t_k)$ by the respective error $\delta\psi_{\text{FB}}(t_k)$ and $\delta\psi_{\text{res}}(t_k)$ at time t_k.

The three plots on the right of Fig. 9 show the iteration–error curves for all 500 time steps. The three plots on the left illustrate the average values of the solver error μ_{FB}, μ_{res}, and μ_{e} as well as the upper and lower error limits given by the average plus or minus the standard deviation of the solver error $\mu_{\text{FB}} \pm \sigma_{\text{FB}}$, $\mu_{\text{res}} \pm \sigma_{\text{res}}$, and $\mu_{\text{e}} \pm \sigma_{\text{e}}$. The latter visualizes the amount of variation of the solver errors over the time steps. The small vertical gap between the averages μ_{FB}, μ_{res}, as well as μ_{e} and the upper and lower limits $\mu_{\text{FB}} \pm \sigma_{\text{FB}}$, $\mu_{\text{res}} \pm \sigma_{\text{res}}$, as well as $\mu_{\text{e}} \pm \sigma_{\text{e}}$ indicates that

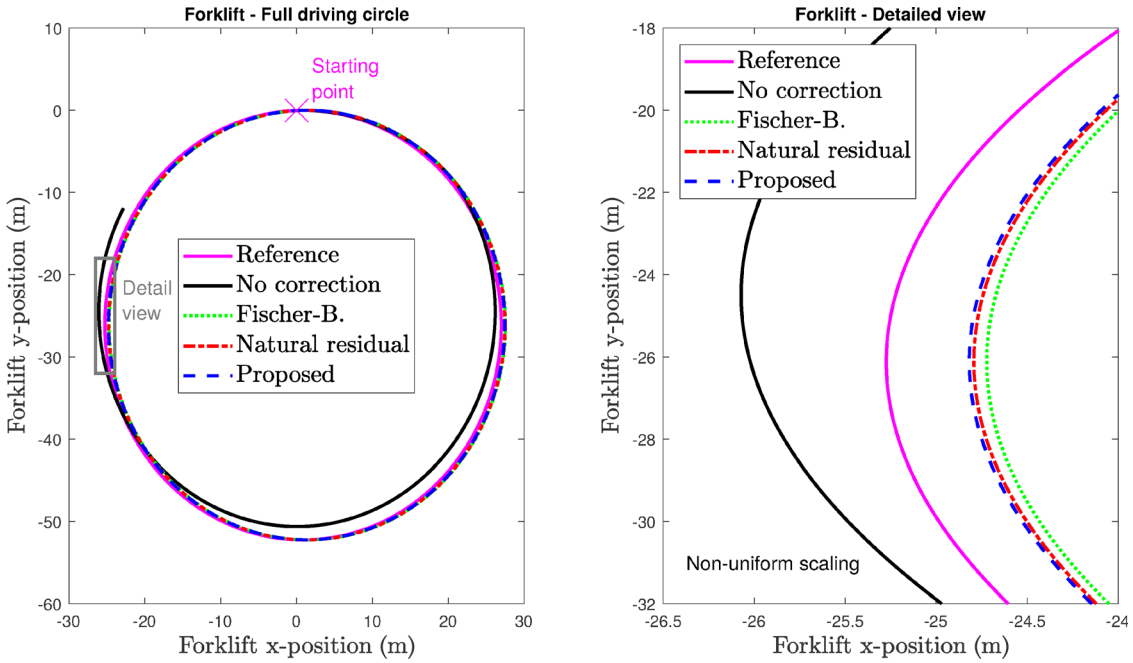

Fig. 11 No error correction, i.e., keeping the last incorrect algorithm solution, leads to a significant offset from the reference trajectory (left). The proposed energy error is closest to the reference trajectory (right).

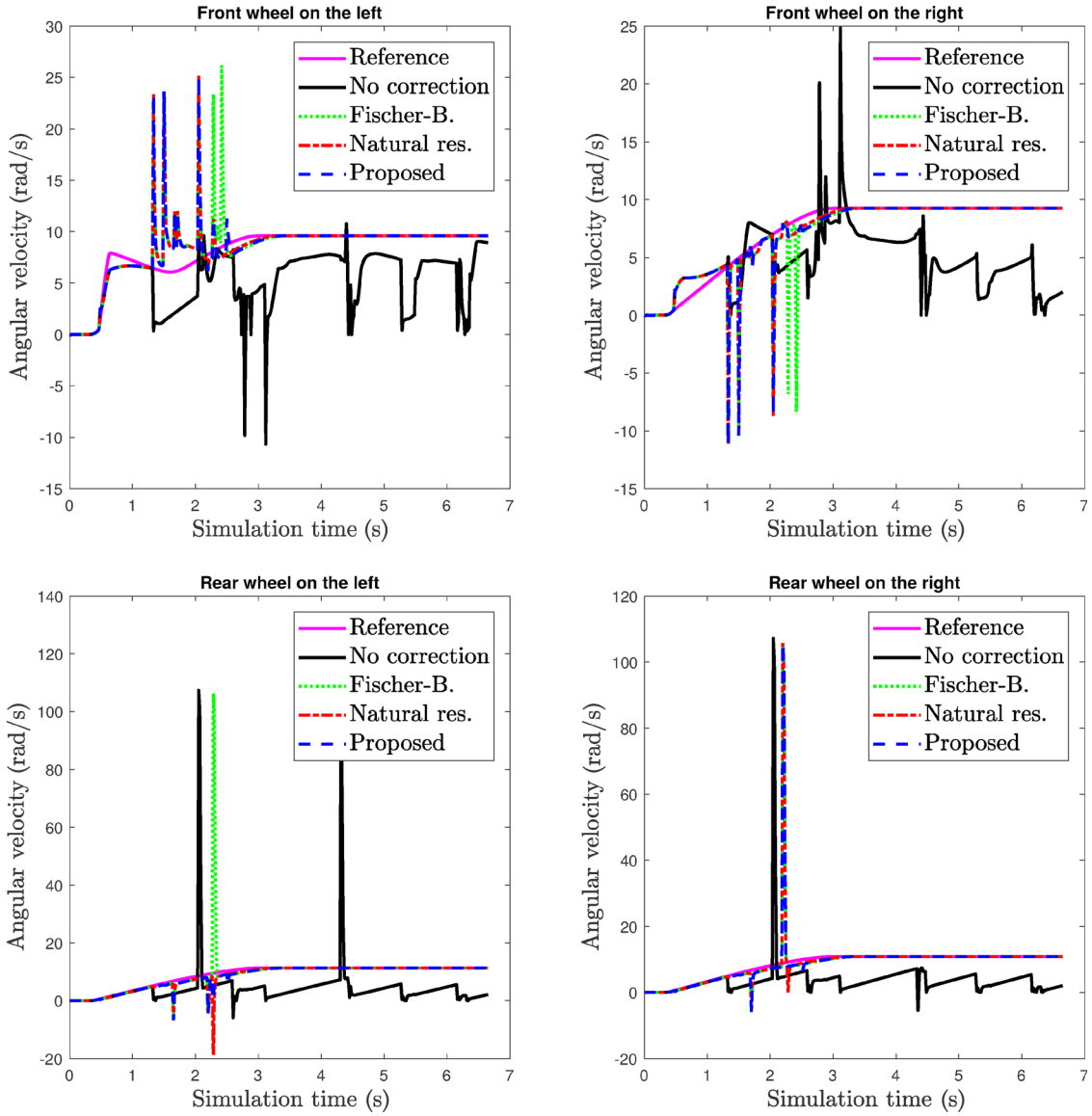

Fig. 12 Angular velocity of the front wheel on the left (top left), the front wheel on the right (top right), the rear wheel on the left (bottom right), and the rear wheel on the right (bottom right). Choosing the best solution based on an error measure significantly reduces velocity instabilities in the simulation. The velocity spikes stop after less than 3 s, whereas the spiky behavior continues past 7 s if the last incorrect algorithm solution is used.

the variation of the solver errors is relatively small for the different time steps as expected for a motionless example. For the error curves of the Fischer-Burmeister and the natural residual error measures, the solver error increases in the first ten iterations, reaches a maximum, and then decreases exponentially with the iteration count. The error curves for the energy error measure do not show any error increase in the first ten iterations, which is more realistic for a convergent iterative solver. Moreover, the exponential decay is steeper than for the other error measures. This is apparent since the energy error decreases quadratically with w_i and x_i, whereas the Fischer-Burmeister and the natural residual error descend linearly with w_i and x_i.

On the right of Fig. 9, we observe that all error curves start from similar error values, which then diverge from each other with an increasing number of iterations. The iterative PGS solver is initialized with the same value $\boldsymbol{\lambda} = \mathbf{0}$ for all time steps, i.e., it is not warm started using the solution of the last time-step. Thus, the error value is similar in the first iteration of each time-step before it converges toward zero error at varying rates. The solution for zero error is not the same for all MLCPs due to numerical instabilities in the brick wall simulation. Note that the accuracy level obtained by the PGS solver would not be sufficient to keep the brick wall permanently stable. It would take several hundred iterations to maintain stability long term. However, the objective of this example is not to present accurate simulation results for a stable brick wall simulation but merely to show that the solver error decreases with the iteration count for the novel unit-consistent measure.

5.3 Continuous Simulation: Driving Forklift. In this example, we test the proposed error measure in a real-time dynamics simulation of a complex mechanical system. A direct block pivoting algorithm [29] is used to compute the constraint, contact, and friction impulses, which are the unknowns of the MLCP formulated for each time-step of the simulation. This algorithm is proven to converge to the exact solution in a finite number of iterations. However, convergence cannot be guaranteed if the number of iterations is limited; as it is often the case for large scale real-time simulations, where a computational-time budged is

imposed for each time-step. For this purpose, we compute the MLCP error for the intermediate solution in each solver iteration using the Fischer-Burmeister, the natural residual, and the proposed energy error measure. If the algorithm does not find the solution in this iteration limit, we either keep the result of the last iteration or choose the intermediate solution with the lowest error according to one of the three error measures in this paper. The generalized velocities and system configuration are then computed based on these constraint impulses.

The forklift in Fig. 10 is modeled using revolute joints for the rotational degree-of-freedom of each wheel. The rear wheels are steerable and controlled by a position input through a revolute joint with limits. We model the rolling resistance of the wheels as angular friction around the axis passing through the two contact points that are used to represent the contact between each wheel and the ground. The drivetrain contains a torque converter between engine and transmission and a differential to allow the two driven front wheels to spin at different speeds. During the simulation, the torque applied to the driven wheels is first increased and then kept constant while the steering angle is kept constant. The vehicle is expected to reach a constant speed in a circular trajectory until it returns to the starting point. We set the iteration limit to 15, which is lower than required to simulate the forklift in real time at 60 Hz. In this case, the MLCP solver is not always able to find the right solution within this artificially small iteration limit.

At first, we create the reference trajectory of the forklift in the x–y-plane using the direct solver without any iteration limit. Then, we repeat the same simulation using a direct solver while enforcing the iteration limit. We monitor the MLCP error for all intermediate solutions and either keep the solution of the last iteration, i.e., no error correction, or pick the one with the lowest error according to the Fischer-Burmeister function, the natural residual, or the proposed energy error measure. Figure 11 shows the forklift trajectories for all five cases. On the left of Fig. 11, the plot of the full driving circle illustrates that the forklift deviates significantly from its path if we simply keep the solution of the last iterate (see curve "no correction"). We can observe multiple discontinuities in the angular speed of the forklift wheels during the first quarter of the driving circle (see Fig. 12), which can be visually perceived as "jerks" in the simulation graphics. This causes the forklift to decelerate temporarily so that it will only travel through about 7/8 of the entire circle at the same time the reference completes the full circle. If we choose the best solution according to one of the error measures, we obtain visually identical solutions compared to the reference. Figure 12 shows that the spikes in the angular velocities of the wheels stop much earlier in the simulation when using an error measure. On the right of Fig. 11, a detailed view of parts of the driving circle is displayed, which shows that the proposed energy error measure is closest to the reference. However, the Fischer-Burmeister and the natural residual based measure are only a few centimeters away.

This forklift example shows that it is definitely advisable to choose the best solution using an error measure since this can prevent large simulation errors that make the forklift diverge from its reference path and even manifest themselves visually. Macroscopically, all three error measures prevent visual differences, abrupt changes in the wheel velocities, and large perturbation from the reference. The proposed energy error leads to a position trajectory closest to the reference trajectory, but only slightly closer than the other two measures. The proposed energy error measure and the natural residual lead to the least wheel velocity fluctuations. However, only the energy error measure provides a physical error interpretation and a unit-consistent treatment of errors.

6 Conclusion

The most used error measures for MLCP solvers do not take the physical nature of mechanical models into account, which leads to an inconsistent treatment of units. The proposed unit-consistent error measure defines an energy error per constraint by means of the effective mass, which solves the unit consistency issue through the transformation of impulse and velocity errors into energy errors. We have shown that only the energy error measure computes the solver error in a unit-consistent manner and it reaches zero error if and only if a valid solution to the MLCP is found. The unit-consistent measure does not require any reference solution, which is a major advantage since it can be costly to compute a reference for large-scale problems. Furthermore, simulation results illustrate that the energy error can decrease monotonically when the MLCP solver converges to the solution. The computational cost of the novel error measure is inexpensive in comparison to the overall cost of an MLCP solver iteration of direct solvers. Thus, the computation can be done for real-time simulations without affecting the performance noticeably. If a direct solver is not able to terminate due to a time constraint, we can monitor all the iterations, determine the solution with the least energy error, and use this solution for further calculations. Simulation results show that using an error measure to monitor the quality of intermediate solutions throughout the algorithm iterations as well as choosing the best solutions among them can significantly reduce the risk of simulation instabilities and deviation from the reference. Moreover, the proposed energy error measure performs best compared to existing error measures or not using any error measure.

As future work, the unit-consistent error could be used to stop the MLCP solver if a solution of the MLCP is found, which is close enough to the true solution. This requires the definition of an error threshold, which classifies what solution will be considered as close enough to the true one and which therefore affects the solution accuracy. It is particularly challenging since the required accuracy of a solution depends on the engineering application and the simulation scenario.

Acknowledgment

This work was supported by the National Science and Engineering Research Council of Canada and CM Labs Simulations, Inc. The authors would like to thank Dr. Francisco González from Laboratorio de Ingeniería Mecánica of University of A Coruña, Prof. Sheldon Andrews from the Department of Software and IT Engineering at École de Technologie Supérieure, and the anonymous reviewers for their advice regarding the measurement of errors in multibody dynamics simulations.

Appendix: Proof on Diagonal Matrix Elements

If matrix $\mathbf{A}$ is symmetric positive definite, then there exists a symmetric positive definite matrix $\mathbf{B}$ such that $\mathbf{A} = \mathbf{B}^2$. The diagonal elements of $\mathbf{A}$ are given as

$$\mathbf{A}_{ii} = \mathbf{e}_i^{\mathrm{T}}\mathbf{A}\mathbf{e}_i = \mathbf{e}_i^{\mathrm{T}}\mathbf{B}^{\mathrm{T}}\mathbf{B}\mathbf{e}_i = ||\mathbf{B}\mathbf{e}_i||^2 \tag{A1}$$

and similarly the diagonal elements of $\mathbf{A}^{-1}$ as $(\mathbf{A}^{-1})_{ii} = ||\mathbf{B}^{-1}\mathbf{e}_i||^2$. The Cauchy–Schwarz inequality leads to

$$\langle \mathbf{B}\mathbf{e}_i, \mathbf{B}^{-1}\mathbf{e}_i \rangle^2 \leq ||\mathbf{B}\mathbf{e}_i||^2 ||\mathbf{B}^{-1}\mathbf{e}_i||^2 = \mathbf{A}_{ii}(\mathbf{A}^{-1})_{ii} \tag{A2}$$

and

$$\langle \mathbf{B}\mathbf{e}_i, \mathbf{B}^{-1}\mathbf{e}_i \rangle = \mathbf{e}_i^{\mathrm{T}}(\mathbf{B}^{-1})^{\mathrm{T}}\mathbf{B}\mathbf{e}_i = \mathbf{e}_i^{\mathrm{T}}\mathbf{B}^{-1}\mathbf{B}\mathbf{e}_i = \mathbf{e}_i^{\mathrm{T}}\mathbf{e}_i = 1 \tag{A3}$$

Thus, it follows that $\mathbf{A}_{ii}(\mathbf{A}^{-1})_{ii} \geq 1$, i.e., the diagonal elements of the inverse of $\mathbf{A}$ are greater than or equal to the inverse of the diagonal elements of $\mathbf{A}$.

References

[1] Júdice, J. J., 1994, "Algorithms for Linear Complementarity Problems," *Algorithms for Continuous Optimization*, E. G. Spedicato, ed., Springer, Dordrecht, The Netherlands, pp. 435–474.

[2] González, M., Dopico, D., Lugrís, U., and Cuadrado, J., 2006, "A Benchmarking System for MBS Simulation Software: Problem Standardization and Performance Measurement," Multibody Syst. Dyn., **16**(2), pp. 179–190.
[3] González, F., Naya, M. Á., Luaces, A., and González, M., 2011, "On the Effect of Multirate Co-Simulation Techniques in the Efficiency and Accuracy of Multibody System Dynamics," Multibody Syst. Dyn., **25**(4), pp. 461–483.
[4] Erez, T., Tassa, Y., and Todorov, E., 2015, "Simulation Tools for Model-Based Robotics: Comparison of Bullet, Havok, Mujoco, ODE and Physx," IEEE International Conference on Robotics and Automation (ICRA), Seattle, WA, May 26–30, pp. 4397–4404.
[5] Ainsworth, M., and Oden, J., 1997, "A Posteriori Error Estimation in Finite Element Analysis," Comput. Methods Appl. Mech. Eng., **142**(1–2), pp. 1–88.
[6] Babuška, I., and Rheinboldt, W. C., 1978, "A-Posteriori Error Estimates for the Finite Element Method," Int. J. Numer. Methods Eng., **12**(10), pp. 1597–1615.
[7] Babuška, I., and Rheinboldt, W. C., 1978, "Error Estimates for Adaptive Finite Element Computations," SIAM J. Numer. Anal., **15**(4), pp. 736–754.
[8] Gago, J. P. De S. R., Kelly, D. W., and Zienkiewicz, O. C., 1983, "A Posteriori Error Analysis and Adaptive Processes in the Finite Element Method—Part 2 Adaptive Mesh Refinement," Int. J. Numer. Methods Eng., **19**(11), pp. 1621–1656.
[9] Babuška, I., Strouboulis, T., Upadhyay, C., Gangaraj, S., and Copps, K., 1994, "Validation of a Posteriori Error Estimators by Numerical Approach," Int. J. Numer. Methods Eng., **37**(7), pp. 1073–1123.
[10] Ainsworth, M., and Oden, J., 2000, *A Posteriori Error Estimation in Finite Element Analysis*, Wiley, New York.
[11] Szabó, B., and Babuška, I., 2011, *Ška, Introduction to Finite Element Analysis*, Wiley, Chichester, UK.
[12] Pang, J.-S., 1986, "Inexact Newton Methods for the Nonlinear Complementarity Problem," Math. Program., **36**(1), pp. 54–71.
[13] Pang, J.-S., 1997, "Error Bounds in Mathematical Programming," Math. Program., **79**(1–3), pp. 299–332.
[14] Mangasarian, O. L., and Shiau, T.-H., 1986, "Error Bounds for Monotone Linear Complementarity Problems," Math. Program., **36**(1), pp. 81–89.
[15] Mangasarian, O. L., and Ren, J., 1994, "New Improved Error Bounds for the Linear Complementarity Problem," Math. Program., **66**(1–3), pp. 241–255.
[16] Fukushima, M., 1996, "Merit Functions for Variational Inequality and Complementarity Problems," *Nonlinear Optimization and Applications*, G. D. Pillo and F. Giannessi, eds., Springer, Boston, MA, pp. 155–170.
[17] Lacoursière, C., Lu, Y., Williams, J., and Trinkle, J., 2013, "Standard Interface for Data Analysis of Solvers in Multibody Dynamics," Canadian Conference on Nonlinear Solid Mechanics, Montréal, QC, Canada, July 23–26, Paper No. 814.
[18] Williams, J., Lu, Y., Niebe, S., Andersen, M., Erleben, K., and Trinkle, J. C., 2013, "RPI-MATLAB-Simulator: A Tool for Efficient Research and Practical Teaching in Multibody Dynamics," Workshop in Virtual Reality Interactions and Physical Simulation, Lille, France, Nov. 27–29, pp. 71–80.
[19] Silcowitz, M., Niebe, S., and Erleben, K., 2010, "Interactive Rigid Body Dynamics Using a Projected Gauss–Seidel Subspace Minimization Method," International Conference on Computer Vision, Imaging and Computer Graphicsin, Angers, France, May 17–21, pp. 218–229.
[20] Lu, Y., and Trinkle, J., 2015, "Comparison of Multibody Dynamics Solver Performance: Synthetic Versus Realistic Data," ASME Paper No. DETC2015-46276.
[21] Lacoursière, C., Linde, M., Lu, Y., and Trinkle, J., 2015, "A Framework for Data Exchange and Benchmarking of Frictional Contact Solvers in Multibody Dynamics," ECCOMAS Thematic Conference on Multibody Dynamics, Barcelona, Spain, June 29–July 2, pp. 2–3.
[22] Lacoursière, C., 2006, "A Regularized Time Stepper for Multibody Systems," HPC2N, Department of Computing Science, Umeå University, Umeå, Sweden, Technical Report No. UMINF-06.04.
[23] Erleben, K., 2007, "Velocity-Based Shock Propagation for Multibody Dynamics Animation," ACM Trans. Graph., **26**(2), pp. 1–20.
[24] Silcowitz, M., Niebe, S., and Erleben, K., 2009, "Nonsmooth Newton Method for Fischer Function Reformulation of Contact Force Problems for Interactive Rigid Body Simulation," Workshop in Virtual Reality Interactions and Physical Simulation, Karlsruhe, Germany, Nov. 5–6, pp. 105–114.
[25] Lu, Y., Williams, J., Trinkle, J., and Lacoursiere, C., 2014, "A Framework for Problem Standardization and Algorithm Comparison in Multibody System," ASME Paper No. DETC2014-35041.
[26] Khatib, O., 1995, "Inertial Properties in Robotic Manipulation: An Object-Level Framework," Int. J. Rob. Res., **14**(1), pp. 19–36.
[27] Kövecses, J., 2008, "Dynamics of Mechanical Systems and the Generalized Free-Body Diagram—Part 1: General Formulation," ASME J. Appl. Mech., **75**(6), p. 061012.
[28] Ulrich, N., and Kumar, V., 1991, "Passive Mechanical Gravity Compensation for Robot Manipulators," IEEE International Conference on Robotics and Automation (ICRA), Sacramento, CA, Apr. 9–11, pp. 1536–1541.
[29] Júdice, J. J., and Pires, F. M., 1994, "A Block Principal Pivoting Algorithm for Large-Scale Strictly Monotone Linear Complementarity Problems," Comput. Oper. Res., **21**(5), pp. 587–596.